ACS Photonics

Article

pubs.acs.org/journal/apchd5

Nonlinear Beam Shaping with Plasmonic Metasurfaces

Shay Keren-Zur,*[,†,§] Ori Avayu,[†,§] Lior Michaeli,[‡] and Tal Ellenbogen[†]

[†]Department of Physical Electronics, Faculty of Engineering, and [‡]Raymond and Beverly Sackler School of Physics & Astronomy, Tel-Aviv University, Tel-Aviv 6779801, Israel

ABSTRACT: We present here a method for generating second-harmonic beams with tailored beam profiles using nonlinear metasurfaces based on split ring resonators. By manipulating both the phase and the amplitude of the quadratic nonlinear coefficient locally, at the single inclusion level, the emitted second-harmonic wavefront is perfectly controlled. These concepts are demonstrated experimentally by the far-field generation of second-harmonic Airy and vortex beams from nonlinear binary phase computer-generated holograms and the perfect near-field generation of a Hermite−Gauss beam by precise amplitude and phase construction. We believe that these demonstrations open the door to use nonlinear metasurfaces for a variety of integrated nonlinear beam shaping devices.

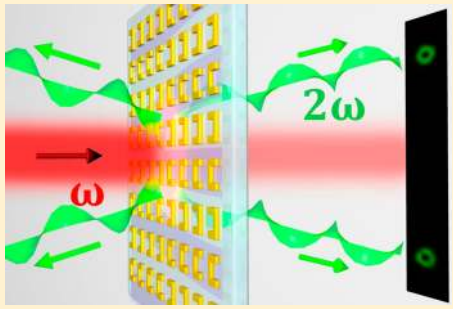

KEYWORDS: *laser beam shaping, metamaterials, nonlinear optical materials, harmonic generation and mixing, photonic crystals*

The wave function of a physical system is of paramount importance with respect to the evolution of its parameters in time and space and to its interaction with other physical systems. In optics, the spatial evolution of the photon wave function can be described by the Helmholtz equation. In the low-light regime its solution gives the spatial photon probabilities, or alternatively, e.g., in the beam optics regime, the solution describes the beam shape. The ability to shape optical beams, from an intense beam down to the single-photon level, can be used to control some of their most important physical parameters, including their orbital angular momentum,[1] spatial intensity, and evolution.[2,3] This enables us to tailor and control the interaction between light and matter. Therefore, beam-shaping techniques are very important and are used across many optical disciplines, e.g., optical tweezing,[4,5] microscopy,[6,7] and optical communications.[8]

Most of the beam-shaping techniques rely on linear optical elements such as waveplates, holographic devices, and spatial light modulators. However, beam shaping can also be achieved by controlling nonlinear optical interactions. This adds functionality to the beam-shaping process and permits the exploration of interesting new possibilities, e.g., generating shaped light at new frequencies,[9,10] all-optical mode control,[9,11] and generation of waveform-entangled states.[12]

Until now, nonlinear beam shaping has mainly used modulated quadratic nonlinear optical materials such as ferroelectric crystals. These materials are very useful for large-scale beam-shaping applications. However, they suffer from several major limitations that prevent them, for example, from being used for small-scale or integrated beam-shaping devices. First of all, the integration of these materials in various platforms is challenging.[13] In addition, only the sign of their local nonlinear coefficient can be modulated,[14] and at a limited resolution,[15] so that only the local phase of the nonlinear interaction can be manipulated and that in a very restricted way. Finally the properties of their nonlinear coefficients are restricted by the finite number of naturally found nonlinear optical materials that are in common use.

One promising way to surpass the existing toolbox for nonlinear beam shaping and utilize it for compact, integrated optical systems is to harness artificial nonlinear heterostructures based on plasmonic metamaterials. These materials commonly consist of nanometer-size metallic inclusions, also called "meta-atoms" or "meta-molecules", which are ordered in structured arrays and collectively define effective bulk optical properties, e.g., the index of refraction. The ability to select the chemical composition, geometry, and the spatial arrangement of the "meta-atoms" at will has extended the response of metamaterials and metasurfaces, some of which now exhibit optical behavior beyond what is found in naturally grown materials.[16−18] Such novel properties include magnetism at optical frequencies and negative refraction, which have been exploited in new functionalities.[19]

In the context of quadratic nonlinear optical interactions, plasmonic metasurfaces were shown to introduce new ways to enable and enhance the quadratic nonlinearity. The enhanced quadratic nonlinearities occur due to the combination of a microscopic symmetry break at the surfaces of the metallic inclusions, coupling of generated plasmonic currents to bright radiating modes, and field confinement associated with excitation of plasmonic modes. These effects were studied in several theoretical and experimental works using different types of metallic inclusions including split ring resonators (SRRs),[20−22] L-shaped[23] and T-shaped[24] inclusions, imperfect spheres,[25] noncentrosymmetric T-shaped nanodimers,[26] and nanotriangles.[27] In addition it was demonstrated that hybrid metasurfaces on top of quantum well structures can be used to harness nonlinear quadratic coefficients that are up to 4 orders

Received: September 17, 2015

DOI: 10.1021/acsphotonics.5b00528
ACS Photonics XXXX, XXX, XXX−XXX

of magnitude larger than conventional nonlinear quadratic materials.[28−30] In addition to enhancement of the local optical nonlinearity, controlling the macroscopic structure of the nonlinear metasurfaces[31−36] can be used to obtain nonlinear diffraction, all-optical control, beam steering, and strong nonlinear focusing.

In this study, we experimentally demonstrate nonlinear beam shaping by exploiting the ability to tailor both the local phase and the amplitude of the nonlinear coefficients of plasmonic metasurfaces in a precise manner. We start by demonstrating that it is possible to use binary manipulations of the local phase of the nonlinear signal to encode nonlinear computer-generated holograms (NL-CGH) in the metasurface. This permits the generation of the desired beam at the Fourier plane (or optical far field). This ability is specifically demonstrated by the nonlinear generation of second-harmonic Airy and vortex beams. In addition, a more comprehensive method for beam shaping is presented. By controlling also the local amplitude of the nonlinear quadratic tensor element, the exact mode of the beam can be generated right after the metasurface (at the so-called optical near field). This ability is demonstrated experimentally by the generation of a first-order Hermite−Gaussian mode (HG_{01}).

BEAM SHAPING BY BINARY PHASE NONLINEAR METASURFACES

The concept of 2D nonlinear beam shaping by NL-CGH in poled ferroelectric crystals was introduced by Shapira et al.[10] based on the Lee method.[37] To encode a desired beam at the output of the nonlinear process in a metasurface, the modulation of the sign of the nonlinear coefficient follows

$$\chi_{\mathrm{eff}}^{(2)}(x, y) = \chi^{(2)}\,\mathrm{sign}\left\{\cos\left[\frac{2\pi x}{\Lambda} - \varphi(x, y)\right] - \cos[\pi q(x, y)]\right\} \tag{1}$$

where x and y are the spatial coordinates, $\chi^{(2)}$ is the magnitude of the bulk quadratic nonlinear coefficient, Λ is the spatial carrier frequency modulation period, $\varphi(x, y)$ encodes the phase of the Fourier transform of the desired wavefront, and $q(x, y)$ encodes its amplitude, A, according to the relation $A(x, y) = \sin[\pi q(x, y)]$). For the case of phase encoding only, the binary modulation in eq 1 can be expanded to a series of harmonic terms with a first-order term equal to

$$\frac{2}{\pi}\exp\left\{\pm i\left[\frac{2\pi}{\Lambda}x - \varphi(x, y)\right]\right\} \tag{2}$$

Therefore, the Fourier transform of the modulated nonlinear coefficient function shows intensity peaks at $k_x = \pm 2\pi/\Lambda$ with the desired waveform.

By shining the NL-CGH with a fundamental beam, $E_{\mathrm{FF}}(x, y)$, the generated second-harmonic (SH) field form is proportional to the quadratic nonlinear coefficient function and the square of the fundamental field:

$$E_{\mathrm{SH}}(x, y) \propto \chi_{\mathrm{eff}}^{(2)}(x, y)\, E_{\mathrm{FF}}(x, y)^2 \tag{3}$$

Assuming an incident plane wave at FF and an infinite size of the metasurface, the optical near field (of the propagating waves) will be proportional to $\chi_{\mathrm{eff}}^{(2)}(x, y)$ and the far field will be proportional to its Fourier transform. The desired beam shape will then be imposed on the first diffraction orders shown in the far field. The angle of emission (defined with respect to the z direction in the x−z plane) and the x direction) to the first diffraction orders obeys momentum conservation in the nonlinear interaction and is given by the Raman−Nath relation:[38]

$$\sin\theta_{\mathrm{SH}} = \frac{\lambda_{\mathrm{FF}}}{2\Lambda} \tag{4}$$

where λ_{FF} is the wavelength of the fundamental frequency.

To use a nonlinear metasurface to construct a binary NL-CGH, it is necessary to control the sign of the local nonlinear coefficient. Using SRRs as the nonlinear building blocks of the metasurface, it is possible to control the sign of the local nonlinear coefficient by simply inverting the orientation of the SRR (Figure 1a and b). This procedure has been employed

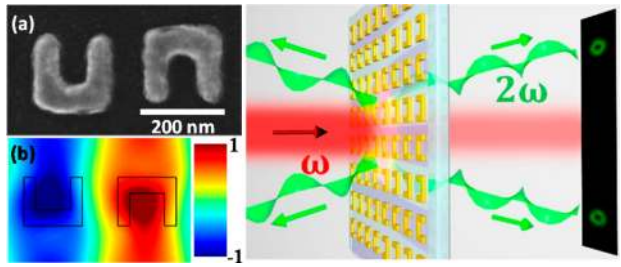

Figure 1. (a) Scanning electron microscope (SEM) image of two gold SRRs with opposite orientation. (b) Simulation of the SH field generated by the SRRs shown in (a), 200 nm above the SRRs. Due to the orientation inversion, each SRR emits SH with an opposite phase (see also Methods). (c) Illustration of NL-CGH for beam shaping. An incident FF beam (red) passes through the metasurface, and SH vortex beams (green) are emitted from the front and the back. The screen on the right shows the projected far-field emission pattern of the SH.

previously to demonstrate the concept of metamaterial-based nonlinear photonic crystals.[32] In contrast to conventional nonlinear materials,[10] the beams are generated in both the forward and backward Fourier planes of the metasurface, as illustrated in Figure 1c, due to the truly 2D nature of the nonlinear metasurface, which eliminates longitudinal phase matching effects.

Here we use the method to demonstrate nonlinear beam shaping by metasurface-based NL-CGH and specifically to generate Airy[39] and vortex beams.[1] The Airy waveform is known for the ballistic trajectory of its intensity peaks as the wave propagates and for its "self-healing" and shape-preserving properties.[40] By virtue of these special features, Airy beams have been used for particle manipulation[41] and microscopy[7] among other applications and have been generated previously by several methods, including spatial light modulators,[42] antenna arrays,[43−45] and nonlinear photonic crystals.[9]

Figure 2a presents the NL-CGH required for generating an Airy beam at the SH, which according to eq 1 is described by

$$\chi_{\mathrm{eff}}^{(2)}(x, y) = \chi_{\mathrm{SRR}}^{(2)}\,\mathrm{sign}\left[\cos\left(\frac{2\pi}{\Lambda}x - f_c y^3\right)\right] \tag{5}$$

where $\chi_{\mathrm{SRR}}^{(2)}$ is the averaged nonlinear coefficient over a unit cell of the metasurface (this value depends on the morphology and chemical composition of the SRR and on the fundamental frequency (FF)[22]) and f_c represents a cubic modulation in the transverse direction, which is the main parameter for defining the generated Airy beam characteristics. The Airy beams will be

DOI: 10.1021/acsphotonics.5b00528
ACS Photonics XXXX, XXX, XXX−XXX

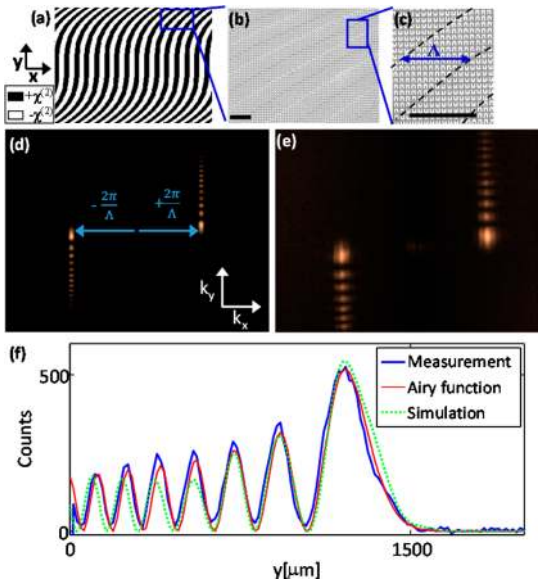

Figure 2. (a) NL-CGH for generation of Airy beams. The black and white areas have nonlinear coefficients with opposite sign. (b) SEM image of part of the fabricated metasurface and (c) magnification of the area showing inversed SRR zones. Scale bars in (b) and (c) are 3 μm. The modulation period of the x-axis is 6.48 μm, and the cubic modulation on the Airy pattern (f_c) is 3.16 × 10^{14} [m^{-3}]. (d) Simulation and (e) measurement of far-field second-harmonic Airy beams at first-order diffractions ($k_x = \pm(2\pi/\Lambda)$). The FF wavelength is 1320 nm. (f) Cross section of the experimentally measured SH Airy beam (blue), compared with a simulation (green) and with the calculated Airy function profile (red). The y-axis shows the size of the beam on the detector.

formed at first-order diffraction lobes of the emission in the optical far field (Fourier plane). This is shown by the beam propagation simulation in Figure 2d. Two Airy beams are formed at the two diffraction orders with opposite shape due to the opposite sign of the phase for the ±1 diffraction terms (eq 2).

Standard e-beam lithography was used to fabricate the metasurface-based NL-CGH from 30 nm thick gold SRRs on top of indium tin oxide coated glass (see Methods). Figure 2b and c show a scanning electron microscope image of part of this structure, where the zones with inverted $\chi^{(2)}_{\mathrm{eff}}$ contain SRRs with opposite orientation. The nonlinear emission was tested in a setup that was described previously,[32] and the measured Fourier plane of the SH beam is shown in Figure 2e for pump wavelength 1320 nm. It can be seen that the emitted SH pattern agrees well with the simulation (see also Figure 2f). The minor discrepancy originates from subtle misalignment of the optical setup and from fabrication imperfections, leading to stretching and appearance of some light at the zeroth-order diffraction in the experiment.

We also designed an NL-CGH that generates vortex beams. These are unique beams whose Poynting vector contains an azimuthal component, resulting in energy flow around a phase singularity in the center of the beam. As a consequence, the beam carries angular orbital momentum[1] and has a ring-shaped intensity profile. The electric field of a vortex beam can be written in cylindrical coordinates as $E(r,\phi,z) = u(r,z)e^{-ikz}e^{il\phi}$, where k is the wavevector and l is an integer that marks the topological charge and indicates phase fronts, which are l intertwined helical surfaces. Each of the photons in the vortex beam carries an orbital angular momentum, which is equal to $\hbar l$. Due to their unique properties, these beams were recently utilized in numerous applications, including optical tweezing[5] and multiplexing in optical communications[8] and for stimulated emission depletion microscopy.[6]

The metasurface-based NL-CGH that we used to generate the vortex beam can be described by[46]

$$\chi^{(2)}_{\mathrm{eff}}(x,\phi) = \chi^{(2)}_{\mathrm{SRR}}\,\mathrm{sign}\left[\cos\left(\frac{2\pi}{\Lambda}x - l\phi\right)\right] \quad (6)$$

where ϕ is the angle relative to the y-axis. The NL-CGH with l = 1 is depicted in Figure 3a, and the simulated and measured

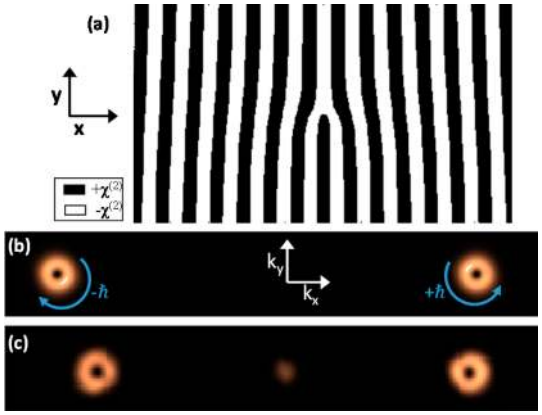

Figure 3. (a) NL-CGH for the generation of vortex beams. (b) Simulation and (c) measurements of SH vortex beams generated at the far field. Each of the vortices carries an opposite angular orbital momentum, of $\pm\hbar$. The FF wavelength is 1320 nm.

SH images in the far field are presented in Figure 3b and c respectively, showing the expected ring shape intensity profile over each of the diffraction orders. Since the opposite diffraction orders have opposite phases as described in eq 2, each of the diffracted vortex beams carries an opposite orbital angular momentum, with the value of $\pm\hbar$.

In order to characterize the emitted SH, we conducted measurements of the dependence of the output beam on the input power, wavelength, and polarization. Figure 4 presents the results for the vortex beam. Figure 4a shows a log–log plot of emitted SH power with respect to the pump power, which gives a slope of ~1.96 (red line), revealing the expected quadratic dependence of the process (deviation from slope of 2 is due to background noise). The dependence of the SH power on the pump polarization is shown in Figure 4b. The maximal output power is obtained when the input polarization is parallel to the base of the SRRs, as was shown previously,[20] and otherwise is decreased proportionally to the fourth power of the dot product between the polarization of the FF and the direction of the base of the SRR, according to $E_{\mathrm{SH}} \propto \chi^{(2)}_{\mathrm{eff}}(E_{\mathrm{FF}}\cos\alpha)^2$ (red line). Additionally, according to eq 4, changing the wavelength of the fundamental beam affects the diffraction angle of the beam, and this is shown experimentally in Figure 4c and d. This ability to scan the vortex beam can be used for active beam tweezing applications.

DOI: 10.1021/acsphotonics.5b00528
ACS Photonics XXXX, XXX, XXX−XXX

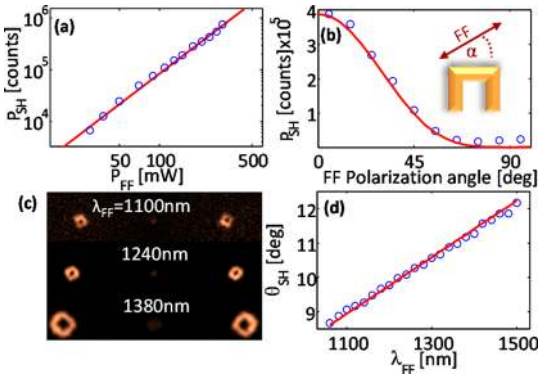

Figure 4. SH beam characterization: (a) Log–log plot of SH beam power vs FF power. (b) SH power dependence on FF polarization angle (α). FF wavelength in (a) and (b) is 1300 nm. (c) Measured SH vortex beams for different FF wavelengths show a different diffraction angle for each FF wavelength, as also presented in (d), where the angle is plotted to show the Raman–Nath relation (eq 4) to the FF wavelength.

BEAM SHAPING BY PHASE AND AMPLITUDE CONTROL OF THE LOCAL QUADRATIC COEFFICIENT

As discussed above, one of the most prominent limitations of conventional quadratic nonlinear materials is that the nonlinear susceptibility is a given fixed property of the material. The current state of the art in this context is to impose local sign changes of $\chi^{(2)}$, e.g., by electric field poling of ferroelectric domains in crystals. Precise local modifications of the nonlinear tensors can pave the way for many new possibilities in general and specifically can facilitate perfect nonlinear beam shaping that cannot be achieved with conventional materials. In this section we demonstrate experimentally that such perfect nonlinear beam shaping can be achieved with nonlinear metasurface-based beam shapers. For demonstration, we present a simple, yet important, example of the generation of a first-order Hermite–Gaussian (HG_{01}) beam by a simple metasurface-based binary modulation (also achievable with conventionally poled ferroelectric crystals), which is compared to a metasurface with locally varying phase and amplitude that forms a perfect beam shaper. This simplified demonstration conveys the idea of perfect mode generation and can be extended to any arbitrary beam shape.

To generate a second-harmonic HG_{01}-like beam at the far field of a binary nonlinear structure, it is possible to shine a Gaussian beam on a structure with the following nonlinear tensor:

$$\chi^{(2)}_{\mathrm{eff}}(x, y) = \chi^{(2)}\mathrm{sign}(x) \quad x \in \left[-\frac{a}{2}, \frac{a}{2}\right] \tag{7}$$

where a is the edge length of the metasurface in the x direction. The SH field in the far field (or Fourier plane) can be expanded to odd HG modes, with a leading term of HG_{01}, but will also contain higher order modes, e.g., HG_{03}, HG_{05}, etc. Since the HG waveforms are eigenmodes of the Helmholtz equation, the ideal way to generate them is to design the metasurface such that it will directly emit into the desired mode, i.e., at the optical near field of propagating waves. The profile of the generated nonlinear SH field by a nonlinear metasurface with a linearly varying quadratic coefficient of the form

$$\chi^{(2)}_{\mathrm{eff}}(x, y) = \frac{2\chi^{(2)}_{\mathrm{max}}}{a}x \quad x \in \left[-\frac{a}{2}, \frac{a}{2}\right] \tag{8}$$

when shined upon with an input FF field with a Gaussian profile, $E_{\mathrm{FF}}(x, y) = E_{\mathrm{FF},0}\, e^{-(x^2+y^2)/2w_0^2}$, ($w_0$ is the beam waist and $\chi^{(2)}_{\mathrm{max}}$) is the maximal nonlinear coefficient), will be, according to eq 3, proportional to:

$$E_{\mathrm{SH}}(x, y) \propto \chi^{(2)}_{\mathrm{max}}\frac{2E^2_{\mathrm{FF},0}}{a}x\,\exp\left[-\frac{(x^2+y^2)}{w_0^2}\right] \tag{9}$$

which follows the HG_{01} profile precisely. The two nonlinear beam-shaping methods are compared in Figure 5, which

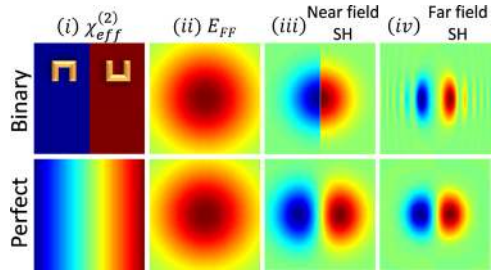

Figure 5. Schemes for the generation of an HG_{01} SH beam by binary modulation (top row) and by perfect beam shaping (bottom row). (i) Effective nonlinear coefficient. (ii) Incident Gaussian beam shape. (iii) Multiplication of the square of the incident Gaussian beam (ii) and the modulation in (i), which gives the generated near-field SH shape. (iv) Corresponding far-field SH.

represents the $\chi^{(2)}_{\mathrm{eff}}$, fundamental beam profile (E_{FF}), optical near-field SH profile, and far-field SH profile, in the panels from left to right, respectively. This demonstrates how the perfect beam-shaping method produces the desired HG_{01} mode already at the optical near field and maintains the shape in the conjugate plane due to its single-mode nature. In contrast, the binary method produces an HG_{01}-like mode only in the far field and also carries energy in the higher order modes as well.

In order to achieve perfect nonlinear beam shaping in the described method, it is necessary to achieve spatial control over the amplitude and sign of the nonlinear coefficient. It was recently reported that the nonlinear properties of SRRs can be accurately predicted using a nonlinear scattering model.[22] It was also shown that the local nonlinear coefficient can be modified by changing the ratio between the length of the arms of the SRRs, L_y, to the total effective length of the SRRs, L_{eff}. The simulated dependence of the nonlinear coefficient strength, $\xi = \chi^{(2)}/\chi^{(2)}_{\mathrm{max}}$, on the ratio L_y/L_{eff} is presented in Figure 6a (see also Methods). Here we use this approach to design metasurfaces with a spatially varying amplitude of the nonlinear coefficient, in order to achieve perfect nonlinear beam shaping of a SH HG_{01} beam, as illustrated in Figure 6b. By spatially designing the SRRs on the metasurface to have an arms-length ratio, which correlates with its location on the x-axis, and by controlling their orientation, it is possible to tailor the entire metasurface to have a quadratic nonlinear coefficient that varies linearly over the x-axis, according to eq 8.

We fabricated two nonlinear beam shaping metasurfaces according to the mentioned methods and examined their performance (see Methods). The simulated and experimental beam-shaping results are shown in Figure 6c. The SH optical near field is presented both by simulations (top) and

DOI: 10.1021/acsphotonics.5b00528
ACS Photonics XXXX, XXX, XXX–XXX

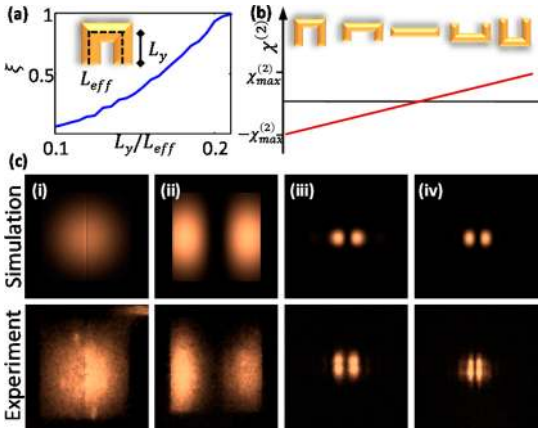

Figure 6. (a) Nonlinear coefficient strength for varying ratios between the length of the arms and the effective length of the SRR, as shown in the inset. (b) Illustration of control of the effective nonlinear coefficient by change of morphology, from $-\chi^{(2)}_{max}$ to $\chi^{(2)}_{max}$. (c) Simulations (top) and measurements (bottom) of SH intensity out of HG_{01} nonlinear beam-shaping metasurfaces. (i) Using binary metasurface and (ii) perfect beam-shaping metasurface. The metasurface size is 100 μm × 100 μm, the incident beam has a waist of 50 μm, and its wavelength is 1100 nm. (iii and iv) Far-field simulations and measurements for (i) and (ii), respectively.

measurements (bottom), with the binary modulation method in part (i) and the perfect beam-shaping method in part (ii). The binary metasurface shows a Gaussian intensity profile, whereas the perfect beam-shaping method clearly shows an HG_{01} intensity profile (truncated by the edges of the metasurface). (iii and iv) Results for the far field of the binary and perfect beam-shaping methods, respectively. In both cases the intensity profile of the beam takes a beam shape that looks like an HG_{01} profile, in both the simulations (top) and measurements (bottom).

The method for perfect shaping of a nonlinear HG_{01} beam, demonstrated here, could also be used for the generation of many other beam profiles and even extended to arbitrary nonlinear holography by metasurfaces.

CONCLUSIONS

In this study, we demonstrate two different methods for nonlinear beam shaping of second-harmonic beams by SRR-based plasmonic metasurfaces. First, by creating metasurface-based NL-CGH we were able to experimentally demonstrate the generation of Airy and vortex beams at the SH and to all-optically scan the output angle by changing the pump wavelength. Additionally we demonstrated perfect beam shaping by precisely tailoring the local quadratic nonlinear tensor to emit the desired beam shape already at the optical near field of the metasurface. In addition to opening the door to perfect nonlinear beam shaping the presented method can be extended to metasurface-based nonlinear holography in general, an achievement not possible with conventional nonlinear materials. The main drawback of the current work is that the total conversion efficiency from nonlinear metasurfaces based on structural nonlinearity is still relatively low. However, with the recent developments of hybrid metasurfaces with giant nonlinearities,[28,29] the results of this work hold great promise for efficient active nonlinear beam shaping over a wide range of optical frequencies and using new integrated platforms.

METHODS

Modeling Second-Harmonic Generation from SRRs. The nonlinear interaction in SRRs was studied using a hydrodynamic model of the free electron in the metal, as was described before (see for example Ciraci et al.[21,47] and references therein). The model was implemented with finite element simulation software (COMSOL Multiphysics), which was used to calculate the SH emission.

The simulation solves the linear polarization that is induced on the SRR at the fundamental frequency. The second-harmonic surface current density on the SRR can then be calculated according to the hydrodynamic model, using the simulated linear polarization. Subsequently, the second-harmonic surface current is fed back into a linear simulation that calculates the nonlinear second-harmonic radiation.

In order to predict the nonlinear coefficient according to the nonlinear scattering model,[22] the overlap integral (OLI) between the three mixed linear modes is calculated by

$$\mathrm{OLI} = \iint E^2_{\mathrm{FF,n}} E_{\mathrm{SH,n}}\, \mathrm{d}S \tag{10}$$

where $E_{\mathrm{FF,n}}$ and $E_{\mathrm{SH,n}}$ are the normal components of linear modes on the surface of the SRR, for the fundamental and second-harmonic frequencies, respectively. These values were also calculated according to numerical simulation using COMSOL Multiphysics. This method was used to design the SRRs and calculate the relative nonlinear coefficient shown in Figure 6a. Optical parameters for gold were taken from Johnson and Christy.[48]

Sample Fabrication. The indium tin oxide coated (15−30 nm thick, 70−100(Ω/sq)) glass substrate was cleaned by acetone and isopropyl alcohol (IPA). The clean substrate was spin-coated with PMMA and baked at 180 °C on a hot plate for 1 min. The metasurface structures were written by an electron beam lithography system (Raith 150) at 10 kV. The patterned substrate was developed by 1:3 methyl isobutyl ketone/IPA for 1 min, followed by rinsing with IPA. An adhesion layer of 2 nm of Ti was evaporated followed by 30/35 nm of Au. The sample was then immersed in acetone for lift-off of the remaining photoresist. For the binary NL-CGH metasurfaces, the SRRs typically had sizes of ∼180 nm base and arm lengths, 50 nm widths, and 30 nm heights. For the perfect nonlinear beam-shaping metasurfaces, the SRRs were 40 nm wide and 35 nm thick with a constant effective length of 270 nm, and with varying arm lengths according to the desired relative efficiency. The spacing between SRRs (resolution) was kept shorter than the wavelength (typically 270 nm) in order to eliminate linear grating effects and to stay in the metamaterial regime for both FF and SH.

Experimental System. A femtosecond optical parametric oscillator (Chameleon OPO VIS, pulse width ∼140 fs, repetition rate 80 MHz) was used as the FF source of a wavelength in the range 1100−1500 nm, chosen as relevant for SHG from the fabricated SRRs, due to a broad SH resonance. Spectral filters were used to avoid residual SH from the OPO, and a half-wave plate and polarizer were used to control the power and polarization of the input FF beam. The beam was focused on the metasurface with a Gaussian profile and a waist of ∼50 μm with a typical average power of 200 mW. The emission from the sample was collected with an objective lens (Mitutoyu NIR X20), filtered spectrally to remove transmitted FF beam, and directed to an imaging spectrometer with a cooled back-illuminated EMCCD detector (Andor Shamrock

DOI: 10.1021/acsphotonics.5b00528
ACS Photonics XXXX, XXX, XXX−XXX

303i, Newton 970). The emission was imaged, either in *k*-space or real space, directly on the CCD. By measuring a uniform array of the fabricated SRRs with the same parameters, the derived value for the quadratic nonlinear coefficient is $\chi^{(2)}_{SRR}$ = 1.36 [pm/V], with a conversion efficiency of 1.6×10^{-11} under these conditions.

AUTHOR INFORMATION

Corresponding Author

*E-mail: shaykerenzur@post.tau.ac.il.

Author Contributions

§S. Keren-Zur and O. Avayu contributed equally.

Notes

The authors declare no competing financial interest.

ACKNOWLEDGMENTS

This research was supported by the Israeli Science Foundation (grant no. 1331/13) and by the European Commission Marie Curie Career Integration Grant (grant no. 333821). S.K. acknowledges support from the Tel-Aviv University Center for Renewable Energy President Scholarship for Outstanding PhD Students.

REFERENCES

(1) Allen, L.; Barnett, S. M.; Padgett, M. J. *Optical Angular Momentum*; CRC Press, 2003.

(2) Dickey, F. M. *Laser Beam Shaping: Theory and Techniques*, 2nd ed.; CRC Press, 2014.

(3) Giovannini, D.; Romero, J.; Poto, V.; Ferenczi, G.; Speirits, F.; Barnett, S. M.; Faccio, D.; Padgett, M. J. Spatially Structured Photons That Travel in Free Space Slower than the Speed of Light. *Science* **2015**, *347*, 857−860.

(4) Dholakia, K.; Čižmár, T. Shaping the Future of Manipulation. *Nat. Photonics* **2011**, *5*, 335−342.

(5) Padgett, M.; Bowman, R. Tweezers with a Twist. *Nat. Photonics* **2011**, *5*, 343−348.

(6) Klar, T. A.; Engel, E.; Hell, S. W. Breaking Abbe's Diffraction Resolution Limit in Fluorescence Microscopy with Stimulated Emission Depletion Beams of Various Shapes. *Phys. Rev. E: Stat. Phys., Plasmas, Fluids, Relat. Interdiscip. Top.* **2001**, *64*, 066613.

(7) Vettenburg, T.; Dalgarno, H. I. C.; Nylk, J.; Coll-Lladó, C.; Ferrier, D. E. K.; Čižmár, T.; Gunn-Moore, F. J.; Dholakia, K. Light-Sheet Microscopy Using an Airy Beam. *Nat. Methods* **2014**, *11*, 541−544.

(8) Wang, J.; Yang, J.-Y.; Fazal, I. M.; Ahmed, N.; Yan, Y.; Huang, H.; Ren, Y.; Yue, Y.; Dolinar, S.; Tur, M.; et al. Terabit Free-Space Data Transmission Employing Orbital Angular Momentum Multiplexing. *Nat. Photonics* **2012**, *6*, 488−496.

(9) Ellenbogen, T.; Voloch-Bloch, N.; Ganany-Padowicz, A.; Arie, A. Nonlinear Generation and Manipulation of Airy Beams. *Nat. Photonics* **2009**, *3*, 395−398.

(10) Shapira, A.; Shiloh, R.; Juwiler, I.; Arie, A. Two-Dimensional Nonlinear Beam Shaping. *Opt. Lett.* **2012**, *37*, 2136−2138.

(11) Ellenbogen, T.; Dolev, I.; Arie, A. Mode Conversion in Quadratic Nonlinear Crystals. *Opt. Lett.* **2008**, *33*, 1207−1209.

(12) Valencia, A.; Ceré, A.; Shi, X.; Molina-Terriza, G.; Torres, J. P. Shaping the Waveform of Entangled Photons. *Phys. Rev. Lett.* **2007**, *99*, 243601.

(13) Guarino, A.; Poberaj, G.; Rezzonico, D.; Degl'Innocenti, R.; Günter, P. Electro−optically Tunable Microring Resonators in Lithium Niobate. *Nat. Photonics* **2007**, *1*, 407−410.

(14) Arie, A.; Voloch, N. Periodic, Quasi-Periodic, and Random Quadratic Nonlinear Photonic Crystals. *Laser Photonics Rev.* **2010**, *4*, 355−373.

(15) Canalias, C.; Pasiskevicius, V. Mirrorless Optical Parametric Oscillator. *Nat. Photonics* **2007**, *1*, 459−462.

(16) Engheta, N.; Ziolkowski, R. W. *Metamaterials*; John Wiley & Sons, Inc.: Hoboken, NJ, USA, 2006.

(17) Cai, W.; Shalaev, V. *Optical Metamaterials*; Springer: New York, NY, 2010.

(18) Yu, N.; Capasso, F. Flat Optics with Designer Metasurfaces. *Nat. Mater.* **2014**, *13*, 139−150.

(19) Minovich, A. E.; Miroshnichenko, A. E.; Bykov, A. Y.; Murzina, T. V.; Neshev, D. N.; Kivshar, Y. S. Functional and Nonlinear Optical Metasurfaces. *Laser Photon. Rev.* **2015**, *9*, 195−213.

(20) Klein, M. W.; Enkrich, C.; Wegener, M.; Linden, S. Second-Harmonic Generation from Magnetic Metamaterials. *Science* **2006**, *313*, 502−504.

(21) Ciracì, C.; Poutrina, E.; Scalora, M.; Smith, D. R. Origin of Second-Harmonic Generation Enhancement in Optical Split-Ring Resonators. *Phys. Rev. B: Condens. Matter Mater. Phys.* **2012**, *85*, 201403.

(22) O'Brien, K.; Suchowski, H.; Rho, J.; Salandrino, A.; Kante, B.; Yin, X.; Zhang, X. Predicting Nonlinear Properties of Metamaterials from the Linear Response. *Nat. Mater.* **2015**, *14*, 379−383.

(23) Kujala, S.; Canfield, B. K.; Kauranen, M.; Svirko, Y.; Turunen, J. Multipole Interference in the Second-Harmonic Optical Radiation from Gold Nanoparticles. *Phys. Rev. Lett.* **2007**, *98*, 167403.

(24) Klein, M. W.; Wegener, M.; Feth, N.; Linden, S. Experiments on Second- and Third-Harmonic Generation from Magnetic Metamaterials. *Opt. Express* **2007**, *15*, 5238−5247.

(25) Nappa, J.; Revillod, G.; Russier-Antoine, I.; Benichou, E.; Jonin, C.; Brevet, P. F. Electric Dipole Origin of the Second Harmonic Generation of Small Metallic Particles. *Phys. Rev. B: Condens. Matter Mater. Phys.* **2005**, *71*, 165407.

(26) Canfield, B. K.; Husu, H.; Laukkanen, J.; Bai, B.; Kuittinen, M.; Turunen, J.; Kauranen, M. Local Field Asymmetry Drives Second-Harmonic Generation in Non-Centrosymmetric Nanodimers. *Nano Lett.* **2007**, *7*, 1251−1255.

(27) Salomon, A.; Zielinski, M.; Kolkowski, R.; Zyss, J.; Prior, Y. Size and Shape Resonances in Second Harmonic Generation from Silver Nanocavities. *J. Phys. Chem. C* **2013**, *117*, 22377−22382.

(28) Lee, J.; Tymchenko, M.; Argyropoulos, C.; Chen, P.-Y.; Lu, F.; Demmerle, F.; Boehm, G.; Amann, M.-C.; Alù, A.; Belkin, M. A. Giant Nonlinear Response from Plasmonic Metasurfaces Coupled to Intersubband Transitions. *Nature* **2014**, *511*, 65−69.

(29) Campione, S.; Benz, A.; Sinclair, M. B.; Capolino, F.; Brener, I. Second Harmonic Generation from Metamaterials Strongly Coupled to Intersubband Transitions in Quantum Wells. *Appl. Phys. Lett.* **2014**, *104*, 131104.

(30) Gomez-Diaz, J. S.; Tymchenko, M.; Lee, J.; Belkin, M. A.; Alù, A. Nonlinear Processes in Multi-Quantum-Well Plasmonic Metasurfaces:Electromagnetic Response, Saturation Effects, Limits and Potentials. *arXiv:1506.07095*, 2015.

(31) Zheludev, N. I.; Emel yanov, V. I. Phase Matched Second Harmonic Generation from Nanostructured Metallic Surfaces. *J. Opt. A: Pure Appl. Opt.* **2004**, *6*, 26−28.

(32) Segal, N.; Keren-Zur, S.; Hendler, N.; Ellenbogen, T. Controlling Light with Metamaterial-Based Nonlinear Photonic Crystals. *Nat. Photonics* **2015**, *9*, 180−184.

(33) Wolf, O.; Campione, S.; Benz, A.; Ravikumar, A. P.; Liu, S.; Luk, T. S.; Kadlec, E. A.; Shaner, E. A.; Klem, J. F.; Sinclair, M. B.; et al. Phased-Array Sources Based on Nonlinear Metamaterial Nanocavities. *Nat. Commun.* **2015**, *6*, 7667.

(34) Kolkowski, R.; Petti, L.; Rippa, M.; Lafargue, C.; Zyss, J. Octupolar Plasmonic Meta-Molecules for Nonlinear Chiral Watermarking at Subwavelength Scale. *ACS Photonics* **2015**, *2*, 899−906.

(35) Almeida, E.; Shalem, G.; Prior, Y. Nonlinear Phase Control and Anomalous Phase Matching in Plasmonic Metasurfaces. *arXiv:1505.05618*, 2015.

(36) Li, G.; Chen, S.; Pholchai, N.; Reineke, B.; Wong, P. W. H.; Pun, E. Y. B.; Cheah, K. W.; Zentgraf, T.; Zhang, S. Continuous Control of the Nonlinearity Phase for Harmonic Generations. *Nat. Mater.* **2015**, *14*, 607−612.

DOI: 10.1021/acsphotonics.5b00528
ACS Photonics XXXX, XXX, XXX−XXX

(37) Lee, W. H. Binary Computer-Generated Holograms. *Appl. Opt.* **1979**, *18*, 3661−3669.
(38) Sheng, Y.; Kong, Q.; Wang, W.; Kalinowski, K.; Krolikowski, W. Theoretical Investigations of Nonlinear Raman−Nath Diffraction in the Frequency Doubling Process. *J. Phys. B: At., Mol. Opt. Phys.* **2012**, *45*, 055401.
(39) Siviloglou, G. A.; Christodoulides, D. N. Accelerating Finite Energy Airy Beams. *Opt. Lett.* **2007**, *32*, 979.
(40) Broky, J.; Siviloglou, G. A.; Dogariu, A.; Christodoulides, D. N. Self-Healing Properties of Optical Airy Beams. *Opt. Express* **2008**, *16*, 12880−12891.
(41) Baumgartl, J.; Mazilu, M.; Dholakia, K. Optically Mediated Particle Clearing Using Airy Wavepackets. *Nat. Photonics* **2008**, *2*, 675−678.
(42) Siviloglou, G. A.; Broky, J.; Dogariu, A.; Christodoulides, D. N. Observation of Accelerating Airy Beams. *Phys. Rev. Lett.* **2007**, *99*, 213901.
(43) Avayu, O.; Eisenbach, O.; Ditcovski, R.; Ellenbogen, T. Optical Metasurfaces for Polarization-Controlled Beam Shaping. *Opt. Lett.* **2014**, *39*, 3892−3895.
(44) Avayu, O.; Epstein, I.; Eizner, E.; Ellenbogen, T. Polarization Controlled Coupling and Shaping of Surface Plasmon Polaritons by Nanoantenna Arrays. *Opt. Lett.* **2015**, *40*, 1520−1523.
(45) Chremmos, I. D.; Fikioris, G.; Efremidis, N. K. Accelerating and Abruptly-Autofocusing Beam Waves in the Fresnel Zone of Antenna Arrays. *IEEE Trans. Antennas Propag.* **2013**, *61*, 5048−5056.
(46) Bloch, N. V.; Shemer, K.; Shapira, A.; Shiloh, R.; Juwiler, I.; Arie, A. Twisting Light by Nonlinear Photonic Crystals. *Phys. Rev. Lett.* **2012**, *108*, 233902.
(47) Ciracì, C.; Poutrina, E.; Scalora, M.; Smith, D. R. Second-Harmonic Generation in Metallic Nanoparticles: Clarification of the Role of the Surface. *Phys. Rev. B: Condens. Matter Mater. Phys.* **2012**, *86*, 115451.
(48) Johnson, P. B.; Christy, R. W. Optical Constants of the Noble Metals. *Phys. Rev. B* **1972**, *6*, 4370−4379.

DOI: 10.1021/acsphotonics.5b00528
ACS Photonics XXXX, XXX, XXX−XXX